Transition in the axisymmetric jet

By BRIAN J. CANTWELL

Department of Aeronautics and Astronautics, Stanford University, Ca. 94305

The unsteady laminar flow from a point source of momentum is considered. Dimensional considerations lead to a formulation of the problem which is self-similar in time. Three limiting cases are examined. In the limit $t \to \infty$ the solution corresponds to the classic steady solution first discovered by Landau (1944). The limit $t \to 0$ was examined recently by Sozou & Pickering (1977) and was shown to correspond to the flow from an unsteady dipole of linearly increasing strength. More recently Sozou (1979) determined an analytic solution for the creeping flow limit $Re \to 0$. In the present work, unsteady particle trajectories for each of these cases are examined by reducing the particle path equations to an autonomous system with the Reynolds number as a parameter. Transition of the jet is examined as a bifurcation of this system. In the case of the creeping-flow solution, the particle-path pattern exhibits a structure which is not easily discerned in any of the other variables which govern the flow. For sufficiently small Reynolds number the particle paths converge to a single stable node which lies on the axis of the jet. At a Reynolds number of 6·7806 the pattern bifurcates to a saddle lying on the axis of the jet plus two stable nodes lying symmetrically to either side of the axis. At a Reynolds number of 10·09089 the pattern bifurcates a second time to form a saddle and two stable foci.

1. Introduction

Transition in fluid flow may occur in a variety of ways but in general two basic types may be distinguished. The first, and by far the most common type, is transition to turbulence. The classic and technologically most important case is that of the flat-plate boundary layer investigated by Schubauer & Skramstad (1947). Here, as in other cases where transition leads to turbulence, the streamwise increase of Reynolds number leads to a succession of instabilities, first linear, then nonlinear, which give rise to a motion which is ultimately chaotic; the flow, which is initially stable and steady, becomes unstable and unsteady as the Reynolds number is increased.

The second type of transition is one where, by variation of the Reynolds number, a flow which is steady and stable is replaced abruptly by a new flow which is also steady and stable. The classic case here is that of circular Couette flow. This was studied by Taylor (1923) and more recently by Coles (1965), who documented a very complex set of stages through which the laminar flow may pass before becoming turbulent. This type of transition has been the subject of renewed interest in recent years (Fenstermacher, Swinney & Golub 1979; Benjamin 1978) partly for its own sake, and partly because it is felt that an increased understanding of transition of the second type will lead to an increased understanding of transition to turbulence.

In the present work we consider the flow produced by an axisymmetric jet emanating

from a point source of momentum with strength J/ρ. As the Reynolds number, $[J/\rho]^{\frac{1}{2}}/\nu$, is increased the flow pattern of the jet undergoes a sequence of regular changes, each of which occurs at a specific critical value of the Reynolds number. In this sense, transition in the jet is reminiscent of transition in couette flow.

The impulsively started axisymmetric jet has been treated numerically on two previous occasions. Ma & Ong (1971) formulated the self-similar problem in cylindrical co-ordinates $(r/(\nu t)^{\frac{1}{2}}, z/(\nu t)^{\frac{1}{2}}, \theta)$ and carried out a finite difference calculation with the primary aim of computing the propagation of the jet front into stagnant fluid. Sozou & Pickering (1977) computed the same flow in spherical self-similar co-ordinates $((\nu t)^{\frac{1}{2}}/r, \theta)$. They noted that for large time, the solution corresponds to the classic steady solution due to Landau (1944) and Squire (1951). Whereas, for small time, the solution corresponds to the flow from an unsteady dipole. They noted further that the streamlines of the developing flow form closed loops about a stagnation point which propagates to infinity along a straight line emanating from the origin. Sozou & Pickering carried out their computations for jet Reynolds numbers in the range $2 \cdot 15 \leqslant [J/\rho]^{\frac{1}{2}}/\nu \leqslant 12 \cdot 5$. At the lower end of this range the streamline pattern of the jet is nearly symmetrical about the equatorial plane $\cos\theta = 0$ and the stagnation point propagates along a line which is nearly 90° away from the direction of the applied force. As the Reynolds number is increased, the streamline pattern develops an asymmetry about the equatorial plane so that at $Re = 12 \cdot 5$ the stagnation point propagates along a line which is about 50° away from the direction of the applied force. More recently, Sozou (1979) re-examined the low-Reynolds-number case and found an analytic solution for the creeping unsteady jet which is uniformly valid for all time.

The stability of the steady axisymmetric jet was analysed by Batchelor & Gill (1962). They examined the inviscid stability of the velocity profile corresponding to the high-Reynolds-number limit of the Landau–Squire solution. Using the usual approximations of parallel flow and infinitesimal disturbances, they found that in the case of a jet with a 'far-downstream' profile only a sinuous helical mode, with axial wavelength several times the jet diameter, can yield amplified disturbances in an inviscid fluid. Their analysis did not yield a value for the critical Reynolds number of the jet.

Observations of a small diameter jet of water into water were made by Viilu (1962) using an acid base reaction and a phenolphthalein indicator for flow visualization. Viilu observed that the jet became unstable at a Reynolds number between 13·1 and 14·75, where the Reynolds number is based on the momentum flux of the jet assuming a parabolic velocity profile at the nozzle exit.† By examining a range of nozzle diameters, Viilu found that the Reynolds number for instability remained roughly constant independent of the diameter of the nozzle. At about the same time, Reynolds (1962) made observations of a jet of dyed water directed into a large tank of water. He observed a variety of modes of instability. At low Reynolds numbers ($10 < Re < 30$) he observed break-up similar to that observed by Viilu. However, as the flow rate was increased, Reynolds noticed that the rapid breakdown at low Reynolds numbers gave way to a progressively longer simple jet which could be maintained up to Reynolds numbers in the range $150 < Re < 300$.

† Viilu reports that stable–unstable transition occurs between a Reynolds number of 10·5 and 11·8 based on the nozzle diameter and the mean velocity obtained from volume flow measurements. He observes that the exit profile must have been close to that of Poiseuille flow, although this was apparently not measured.

In an attempt to explain some of these observations, the analysis of Batchelor & Gill was extended by Gill (1962) to the case where the fluid was slightly viscous and the disturbances were small but finite. He showed that axisymmetric disturbances do not grow in a slightly viscous fluid and suggested that the growth of small but finite disturbances is responsible for the 'condensations' observed experimentally by Reynolds. In the present paper we will study transition of the axisymmetric jet from a rather different point of view. We will examine the unsteady self-similar flow from a starting jet in the creeping flow limit $Re \to 0$. This limiting solution, which is perfectly symmetric about the equatorial plane $\cos\theta = 0$, is shown to have a remarkably complex structure when analysed in terms of non-steady particle paths. The main features of the analysis are:

(i) There is no assumption that the flow is parallel or that it is subjected to small disturbances. The method of analysis, though straightforward, is quite new and lies outside the usual small disturbance theory used to determine the stability of various velocity profile shapes.

(ii) The analysis yields not one but two critical Reynolds numbers for the jet.

(iii) The main results of the present paper are derived from an examination of the creeping-flow solution at Reynolds numbers which lie outside of its region of validity. Nevertheless, the method of approach is essentially nonlinear and can be used to investigate the structure of numerical solutions based on the full equations of motion.

(iv) The flow pattern produced by plotting particle trajectories in similarity co-ordinates is the same for all moving observers who translate (non-uniformly) along a radius at a velocity equal to some constant times $t^{-\frac{1}{2}}$. As a consequence, structural features of the flow are brought out in a simple and invariant way without reference to an observer who might translate with any particular feature. This is in contrast to the pattern of streamlines in physical or similarity co-ordinates which changes when referenced to a moving observer.

2. Statement of the problem

Consider the incompressible flow from a point source of momentum which starts at time $t = 0$ and thereafter exerts a force per unit mass on the fluid which is equal to J/ρ (units length⁴/time²). The governing equations in spherical polar co-ordinates are

$$\frac{1}{r}\frac{\partial}{\partial r}(r^2 u) + \frac{1}{\sin\theta}\frac{\partial}{\partial\theta}(v\sin\theta) = 0 \quad \text{(continuity)}, \tag{1}$$

$$r\omega = \frac{\partial(rv)}{\partial r} - \frac{\partial u}{\partial\theta} \quad \text{(vorticity)}, \tag{2}$$

$$\frac{\partial(r\omega)}{\partial t} + \frac{\partial}{\partial r}(ru\omega) + \frac{\partial}{\partial\theta}(v\omega) = \nu\left\{\frac{1}{r}\frac{\partial}{\partial\theta}\left(\frac{1}{\sin\theta}\frac{\partial}{\partial\theta}(\omega\sin\theta)\right) + \frac{\partial^2}{\partial r^2}(r\omega)\right\} \quad \text{(momentum)}. \tag{3}$$

The Stokes stream function is used to integrate the continuity equation as

$$u = \frac{1}{r^2\sin\theta}\frac{\partial\psi}{\partial\theta}; \quad v = \frac{-1}{r\sin\theta}\frac{\partial\psi}{\partial r}. \tag{4}$$
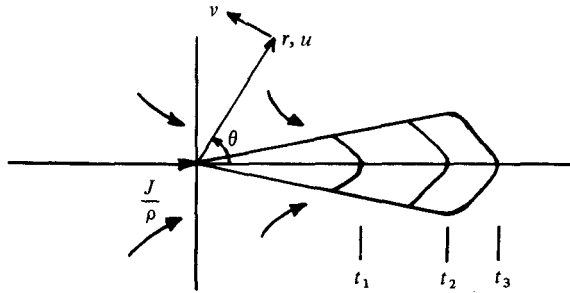
FIGURE 1. Schematic diagram of the unsteady propagation of a started jet.

We will be concerned with the equations for unsteady particle paths given by

$$\frac{dr}{dt} = u, \quad \frac{d\theta}{dt} = \frac{v}{r},$$

(5)

where the velocity components, u and v, are in the radial and tangential directions, respectively.

Dimensional considerations lead to the conclusion that the boundary of the region of disturbed rotational flow (shown schematically in figure 1) must propagate in a geometrically similar way and that any length scale of the jet must vary as $t^{\frac{1}{2}}$. This leads to similarity variables

$$\xi = r/(\nu t)^{\frac{1}{2}}, \theta; \quad \Psi = \nu^{\frac{1}{2}} t^{\frac{1}{2}} g(\xi, \theta),$$

(6)

where ν is the kinematic viscosity, Ψ is the Stokes stream function, and r and θ are the radius and polar angle in spherical co-ordinates.

Upon substitution of (6) the system (1)–(5) becomes

$$\frac{1}{\xi} \frac{\partial}{\partial \xi} (\xi^2 U) + \frac{1}{\sin \theta} \frac{\partial}{\partial \theta} (V \sin \theta) = 0 \quad \text{(continuity)},$$

(7)

$$\omega = \frac{1}{t} W(\xi, \theta), \quad \xi W(\xi, \theta) = \frac{\partial}{\partial \xi} (\xi V) - \frac{\partial U}{\partial \theta} \quad \text{(vorticity)},$$

(8)

$$\frac{\partial}{\partial \xi} \left\{ \left(U - \frac{\xi}{2} \right) (\xi W) \right\} - \frac{\partial}{\partial \theta} \{ V W \} = \frac{\partial^2}{\partial \xi^2} (\xi W) + \frac{1}{\xi} \frac{\partial}{\partial \theta} \left(\frac{1}{\sin \theta} \frac{\partial}{\partial \theta} (W \sin \theta) \right) \quad \text{(momentum)}.$$

(9)

The reduced velocities U and V are given by

$$U(\xi, \theta) = \frac{1}{\xi^2 \sin \theta} \frac{\partial g}{\partial \theta}, \quad V(\xi, \theta) = -\frac{1}{\xi \sin \theta} \frac{\partial g}{\partial \xi},$$

(10)

and the particle path equations (5) become

$$\frac{d\xi}{d\tau} = U(\xi, \theta) - \frac{1}{2}\xi, \quad \frac{d\theta}{d\tau} = \frac{V(\xi, \theta)}{\xi},$$

(11)

where $\tau = \ln t$. The Reynolds number of the jet is

$$Re = [J/\rho]^{\frac{1}{2}}/\nu.$$

(12)

In the following sections we shall consider several solutions to the system (7)–(10). The first will be the classic steady solution due to Landau which, when recast in

unsteady self-similar co-ordinates, forms the boundary condition for the started jet in the limit $\xi \to 0$ $(t \to \infty)$. The second will be the irrotational flow due to a dipole of linearly increasing strength. This forms the boundary condition for the started jet in the limit $\xi \to \infty$ $(t \to 0)$. An important feature of the problem is that, although the reduced system (7)–(10) does not contain the Reynolds number explicitly, the boundary conditions at $\xi \to 0$ and $\xi \to \infty$ do depend on *Re*. A related feature, which is a consequence of the dimensions of J/ρ and ν, is the fact that the Reynolds number does not vary in space. This is in contrast to the boundary layer on a flat plate or, for that matter, the laminar plane jet. This is the key feature of the problem which admits transition which does not necessarily lead to turbulence.

First, particle paths for both the Landau–Squire solution and the unsteady dipole are examined using (11). Then the solution for the limit $Re \to 0$ is examined. In each case the Reynolds number appears in the system (11) as a parameter and the possibility of bifurcation follows.

Transition in the axisymmetric jet differs from transition in Couette flow in that, whereas Couette flow involves a bounded steady flow which bifurcates to a new steady flow, the jet involves an unbounded, unsteady, self-similar flow which bifurcates to a new unsteady self-similar flow.

3. Particle paths – invariance

Much of the analysis which follows will focus on various isocline patterns of (11) and on critical points (ξ_0, θ_0), where

$$U(\xi_0, \theta_0) - \tfrac{1}{2}\xi_0 = 0, \tag{12}$$

and

$$V(\xi_0, \theta_0)/\xi_0 = 0. \tag{13}$$

There are several useful aspects of this approach. Structural features of the flow, which are implicitly contained in a pattern of streamlines are explicitly displayed in a pattern of particle trajectories. Moreover, the pattern of particle trajectories is invariant. To see this it is convenient to consider a general unsteady three-dimensional flow with length scales which grow like $(\nu t)^{\frac{1}{2}}$. The particle-path equations in Cartesian co-ordinates (displacement; x_i, velocity; u_i and vorticity; ω_i, $i = 1, 2, 3$) are

$$\frac{dx_i}{dt} = u_i. \tag{14}$$

Consider a transformation, in Cartesian co-ordinates, to an observer who moves (non-uniformly) outward along a radius with

$$x_i' = x_i - \alpha_i(\nu t)^{\frac{1}{2}}, \quad t' = t, \quad u_i' = u_i - \tfrac{1}{2}\alpha_i(\nu/t)^{\frac{1}{2}}, \quad \omega_i' = \omega_i. \tag{15}$$

In the case of the jet, any structural feature moves along a line $\theta = $ constant and the values of the α_i might be chosen so as to follow a particular feature. In terms of similarity variables $(\xi_i = \nu^{-\frac{1}{2}}t^{-\frac{1}{2}}x_i,\ U_i = \nu^{-\frac{1}{2}}t^{\frac{1}{2}}u_i,\ W_i = t\omega_i)$ the particle-path equations (14) become

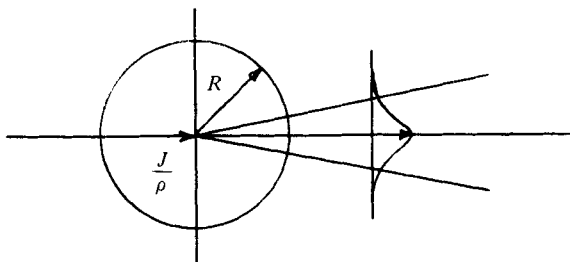$$\frac{d\xi_i}{d\tau} = U_i - \tfrac{1}{2}\xi_i, \tag{16}$$

FIGURE 2. Fixed control volume for a momentum balance at $\xi = 0$.

where $\tau = \ln t$. The transformation (15) becomes a simple translation when cast in terms of similarity variables

$$\xi_i' = \xi_i - \alpha_i, \quad U_i' = U_i - \tfrac{1}{2}\alpha_i, \quad W_i' = W_i. \tag{17}$$

The adjustment of u_i by $\tfrac{1}{2}\alpha_i(\nu/t)^{\frac{1}{2}}$ (or U_i by $\tfrac{1}{2}\alpha_i$) is the property of (15) which causes the velocity vector field to be different for different observers. This is true whether one plots the vector field, u_i, in physical co-ordinates or the vector field, U_i, in similarity co-ordinates. In contrast, if we examine the particle path equations (16) we find $U_i' - \tfrac{1}{2}\xi_i' = U_i - \tfrac{1}{2}\alpha_i - \tfrac{1}{2}(\xi_i - \alpha_i) = U_i - \tfrac{1}{2}\xi_i$. All observers, moving or not, would assign the same numerical values to the components ($d\xi_i$; $i = 1, 2, 3$) of the particle displacement vectors in similarity co-ordinates. A moving observer would assign these values at points which are uniformly displaced by a fixed amount $c = (\alpha_1^2 + \alpha_2^2 + \alpha_3^2)^{\frac{1}{2}}$ along a ray $\theta = $ constant, but this displacement would not affect the pattern of particle trajectories. The implication of this is that the location and character of a critical point in similarity co-ordinates is fixed by the dynamics which govern the flow and not by the incidental choice of speed (which may be zero) for a moving observer. Additional discussion of this invariance, for a flow with length scales which grow like t, may be found in Cantwell, Coles & Dimotakis (1978) where particle trajectories were used to identify critical points in the flow pattern of a turbulent spot.

4. The limit $\xi \to 0$ ($t \to \infty$)

Landau (1944) and, independently, Squire (1951), solved the steady problem of a jet emerging from a point source of momentum which was assumed to have been turned on for all time. The Stokes stream function for this case is

$$\Psi = \nu r \left(\frac{2 \sin^2 \theta}{A - \cos \theta} \right). \tag{18}$$

The constant A is related to the Reynolds number by considering an integral momentum balance over a sphere of fixed radius R (see figure 2).

$$\frac{J}{\rho} = \int_0^\pi \left\{ u(u \cos \theta - v \sin \theta) - \left(\frac{\tau_{rr}}{\rho} \cos \theta - \frac{P}{\rho} \cos \theta - \frac{\tau_{r\theta}}{\rho} \sin \theta \right) \right\} 2\pi R^2 \sin \theta \, d\theta. \tag{19}$$

The stresses τ_{rr}/ρ and $\tau_{r\theta}/\rho$ are related to the velocity field by the usual Newtonian relations

$$\frac{\tau_{rr}}{\rho} = \nu \left(2 \frac{\partial u}{\partial r} \right); \quad \frac{\tau_{r\theta}}{\rho} = \nu \left\{ r \frac{\partial}{\partial r} \left(\frac{v}{r} \right) + \frac{1}{r} \frac{\partial u}{\partial \theta} \right\}. \tag{20}$$

The pressure is related to the velocity field by the r and θ components of the momentum equation. In short, all the terms in (19) can be represented explicitly in terms of r, θ and A, through repeated use of (18). When the integral is carried out the result is

$$\frac{Re^2}{16\pi} = A + \frac{4}{3}\frac{A}{A^2-1} - \frac{A^2}{2}\ln\frac{A+1}{A-1}. \tag{21}$$

Note that as $Re \to 0$; $A \to \infty$ and as $Re \to \infty$; $A \to 1$.

The solution (18) is a perfectly steady flow. However, we can put it in the form (6) by simply multiplying and dividing by $(\nu t)^{\frac{1}{2}}$. We shall take

$$\lim_{\xi \to 0} g(\xi, \theta) = \frac{2\xi \sin^2 \theta}{A - \cos \theta} \equiv g_0(\xi, \theta) \tag{22}$$

as the solution of the impulsively started jet for small ξ. Substitution of (22) into (7)–(10) confirms that (22) is a solution of the governing equations.

5. The limit $\xi \to \infty$ $(t \to 0)$

In the previous section we examined Landau's solution for the steady jet as an unsteady self-similar solution to the system (7)–(10). This solution conserves the flux of momentum from the source at $\xi = 0$ and, at first sight, there would seem to be no reason to go any further. However, we wish to consider a jet which has been turned on for a finite time and therefore has produced a flow field which contains a finite amount of momentum. The solution (22) violates this requirement. The basic requirements at $\xi \to \infty$ are that the solution be irrotational and that it conserve momentum. Sozou & Pickering (1977) showed that, at a fixed radius, the solution for small time corresponds to the flow from an unsteady dipole. The Stokes stream function for this case is

$$\psi = \frac{\nu^2 t}{r}(B \sin^2 \theta). \tag{23}$$

We can put (23) in the form (6) by multiplying and dividing by $(\nu t)^{\frac{1}{2}}$. We shall take

$$\lim_{\xi \to \infty} g(\xi, \theta) = \frac{B \sin^2 \theta}{\xi} = g_\infty(\xi, \theta) \tag{24}$$

as the solution of the impulsively started jet for large ξ.

The dipole (24) is irrotational and thus automatically satisfies (7)–(10). The constant B may be related to the Reynolds number by considering a balance of forces which act on and inside a sphere of radius $R = \xi_c(\nu t)^{\frac{1}{2}}$, where $\xi_c \gg Re^{\frac{1}{2}}/\pi^{\frac{1}{4}}$ and $\xi_c \gg 1$. This condition on ξ_c ensures that, after a time t, the radius R is large compared to either an inertial or a viscous propagation distance. The sphere is an expanding control volume which is located at $\xi = \xi_c = $ constant in similarity co-ordinates (see figure 3). The integral momentum balance is

$$\frac{J}{\rho} = \frac{d}{dt}\int_0^\pi \int_0^R (u\cos\theta - v\sin\theta)\, 2\pi r^2 \sin\theta \, dr \, d\theta + \int_0^\pi \frac{P}{\rho}\cos\theta \, 2\pi R^2 \sin\theta \, d\theta$$

$$+ \int_0^\pi \left(\frac{R}{2t} - u\right)(u\cos\theta - v\sin\theta)\, 2\pi R^2 \sin\theta \, d\theta$$

$$- \int_0^\pi \left(\frac{\tau_{rr}}{\rho}\cos\theta - \frac{\tau_{r\theta}}{\rho}\sin\theta\right) 2\pi R^2 \sin\theta \, d\theta. \tag{25}$$
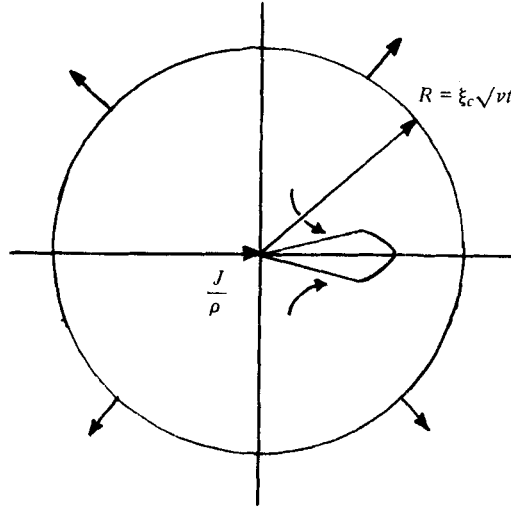
FIGURE 3. Expanding control volume for a momentum balance at $\xi = \infty$.

The first integral above represents the rate of change of total momentum inside the sphere. The third integral is the flux of momentum into the sphere due to the outward movement of the boundary into the fluid. The second and fourth integrals are forces due to pressure and viscosity integrated over the surface of the sphere.

Each of the integrals in (25) is evaluated with u, v, τ_{rr}, $\tau_{r\theta}$ and P determined using $g_\infty(\xi, \theta)$. When the limit $\xi_c \to \infty$ is taken, the third and fourth integrals are zero. The second integral is

$$\int_0^\pi \frac{P}{\rho} \cos\theta \, 2\pi R^2 \sin\theta \, d\theta = \tfrac{4}{3}\pi\nu^2 B. \tag{26}$$

The first integral in (25) requires some care. It involves integrating the solution, which we do not yet know, over the interior of the expanding control volume. Using (4) and (6) we have

$$\frac{d}{dt}\int_0^\pi \int_0^R (u\cos\theta - v\sin\theta)\, 2\pi r^2 \sin\theta \, dr \, d\theta = \nu^2 \int_0^\pi \int_0^{\xi_c} \left[\frac{\partial}{\partial\theta}(g\cos\theta) + \frac{\partial}{\partial\xi}(\xi g \sin\theta)\right] 2\pi \, d\xi \, d\theta. \tag{27}$$

Taking the limit $\xi_c \to \infty$ and making use of the known expressions for g at $\xi \to 0$ and $\xi \to \infty$, plus the fact that $g(\xi, 0) = g(\xi, \pi) = 0$, we have

$$\nu^2 \int_0^\pi \int_0^{\xi_c} \left[\frac{\partial}{\partial\theta}(g\cos\theta) + \frac{\partial}{\partial\xi}(\xi g \sin\theta)\right] 2\pi \, d\xi \, d\theta = \nu^2 \int_0^\pi B\sin^2\theta \, 2\pi \, d\theta = \tfrac{8}{3}\pi\nu^2 B. \tag{28}$$

Combining (26) and (28)

$$B = \frac{J}{4\pi\rho\nu^2} = \frac{Re^2}{4\pi}, \tag{29}$$

in agreement with Sozou & Pickering (1977).

The flow at ∞ is that due to a dipole of strength Jt/ρ. This is also the total impulse applied to the fluid since the initiation of the source. Two-thirds of this impulse is contained in the directed motion of the fluid (28). One third is lost to opposing, unsteady pressure forces which act at ∞ (26).

6. The limit $Re \to 0$

If one takes the limit of (21) as $A \to \infty$ ($Re \to 0$) the result is

$$A = \frac{16\pi}{Re^2}. \tag{30}$$

In this limit the solution near $\xi = 0$ becomes symmetric in θ and one may expect an overall solution of the form

$$\lim_{Re \to 0} g(\xi, \theta) = \epsilon \sin^2 \theta \, F(\xi), \tag{31}$$

where

$$\epsilon = \frac{Re^2}{16\pi}, \tag{32}$$

and

$$\lim_{\xi \to 0} F(\xi) = 2\xi; \quad \lim_{\xi \to \infty} F(\xi) = 4/\xi. \tag{33}$$

Substituting (31) into (8), (9) and (10) and neglecting terms of order ϵ^2, leads to a linear ordinary differential equation for $F(\xi)$. The solution (Sozou 1979) is

$$\lim_{Re \to 0} g(\xi, \theta) = \frac{Re^2}{16\pi} \sin^2 \theta \left\{ 2\xi - \frac{4}{\sqrt{\pi}} e^{-\frac{1}{4}\xi^2} - \left(2\xi - \frac{4}{\xi}\right) \mathrm{erf}\left(\frac{\xi}{2}\right) \right\} \equiv G(\xi, \theta). \tag{34}$$

7. Particle paths – bifurcation

At this point, having dispensed with the system (7)–(10), we will attend to (11) as a nonlinear autonomous set of ordinary differential equations with the Reynolds number as a parameter. For a thorough discussion of bifurcations of nonlinear dynamic systems, see Andronov, Leontovich, Gordon & Maier (1977).

In the neighbourhood of a critical point (ξ_0, θ_0) equations (11) may be expanded as (Perry & Fairlie, 1974)

$$d\xi/d\tau = a(\xi - \xi_0) + b(\theta - \theta_0),$$
$$d\theta/d\tau = c(\xi - \xi_0) + d(\theta - \theta_0). \tag{35}$$

The character of the critical point is completely determined by the negative of the trace $p = -(a+d)$ and determinant $q = ad - bc$ of the matrix of coefficients. Use of the continuity equation (7), vorticity equation (8), and the rate of strain tensor lead to a relationship between the character of a critical point and the strain and vorticity in its neighbourhood. From continuity

$$p = \begin{cases} \frac{3}{2} & (\theta_0 \neq 0) \\ \frac{3}{2} + d & (\theta_0 = 0). \end{cases} \tag{36}$$

From the definitions of vorticity and the rate of strain tensor

$$W(\xi_0, \theta_0) = c\xi_0 - \frac{b}{\xi_0}, \tag{37}$$

$$S_{ij}(\xi_0, \theta_0) = \begin{bmatrix} a + \frac{1}{2} & \frac{1}{2}(\xi_0 c + b/\xi_0) \\ \frac{1}{2}(\xi_0 c + b/\xi_0) & d + \frac{1}{2} \end{bmatrix}. \tag{38}$$
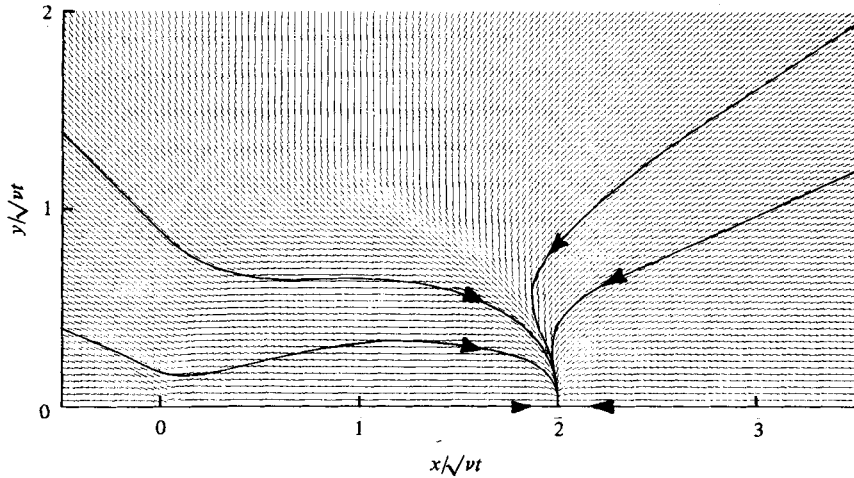
FIGURE 4. Particle trajectories for $g_0(\xi, \theta)$ with $A = 3\cdot0$.

Using (36), (37) and (38)

$$q = \begin{cases} \Omega^2 - S^2 + \tfrac{1}{2} & (\theta_0 \neq 0) \\ \Omega^2 - S^2 + \tfrac{1}{2} + \tfrac{1}{2}d & (\theta_0 = 0), \end{cases} \tag{39}$$

where $\Omega = \tfrac{1}{2}W(\xi_0, \theta_0)$ and $S = (-\det(S_{ij}(\xi_0, \theta_0)))^{\frac{1}{2}}$.

Now consider the particle trajectories and critical points associated with the three functions $g_0(\xi, \theta)$, $g_\infty(\xi, \theta)$ and $G(\xi, \theta)$ repeated below,

$$g_0(\xi, \theta) = \frac{2\xi \sin^2 \theta}{A - \cos \theta}, \tag{40}$$

$$g_\infty(\xi, \theta) = \frac{Re^2}{4\pi} \frac{\sin^2 \theta}{\xi}, \tag{41}$$

$$G(\xi, \theta) = \frac{Re^2}{16\pi} \sin^2 \theta \left\{ 2\xi - \frac{4}{\sqrt{\pi}} e^{-\frac{1}{4}\xi^2} - \left(2\xi - \frac{4}{\xi}\right) \mathrm{erf}\left(\frac{\xi}{2}\right) \right\}. \tag{42}$$

First let us examine the flow pattern of $g_0(\xi, \theta)$. Using the definitions (10), substitute (40) into (11). The result is

$$\frac{d\xi}{d\tau} = \frac{2}{\xi} \left\{ \frac{(A^2 - 1)}{(A - \cos \theta)^2} - 1 \right\} - \frac{\xi}{2}; \quad \frac{d\theta}{d\tau} = \frac{2 \sin \theta}{\xi(A - \cos \theta)}. \tag{43}$$

The system (43) has a single stable node with $p = \tfrac{5}{4}$ and $q = \tfrac{1}{4}$, located at

$$(\xi_0, \theta_0) = (2\sqrt{(2/(A - 1))}, 0).$$

The particle path pattern of (43) with $A = 3\cdot0$ is shown in figure 4. Each of figures 4, 5, 7 and 8 shows particle trajectories in the upper half of the $x/\sqrt{(\nu t)}$, $y/\sqrt{(\nu t)}$ plane.

Now examine the flow pattern of $g_\infty(\xi, \theta)$. Using the definitions (10), substitute (41) into (11). The result is

$$\frac{d\xi}{d\tau} = \frac{Re^2}{2\pi} \frac{\cos \theta}{\xi^3} - \frac{\xi}{2}; \quad \frac{d\theta}{d\tau} = \frac{Re^2}{4\pi} \frac{\sin \theta}{\xi^4}. \tag{44}$$
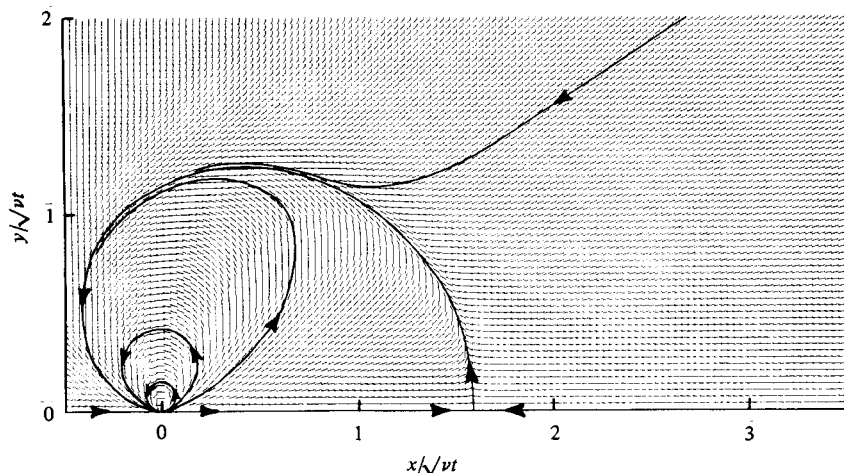
FIGURE 5. Particle trajectories for $g_\infty(\xi, \theta)$ with $R = 4\cdot375$ ($A = 3\cdot0$).

The system (44) has a saddle with $p = \frac{7}{4}$ and $q = -\frac{1}{2}$, located at $(\xi_0, \theta_0) = [(Re^{\frac{1}{2}})/(\pi^{\frac{1}{4}}), 0]$. The particle path pattern of (44) with $Re = 4\cdot375$ ($A = 3\cdot0$) is shown in figure 5.

Figures 4 and 5 provide a useful insight into the structure of the functions $g_0(\xi, \theta)$ and $g_\infty(\xi, \theta)$. While a small area in each figure (near $\xi = 0$ in figure 4 and at large ξ in figure 5) closely approximates the flow from a started jet, the figures are not intended to represent an expansion of $g(\xi, \theta)$ in powers of ξ. They are presented solely as a method of exploring the structure of the flow fields represented by the functions g_0 (Landau–Squire) and g_∞ (unsteady dipole).

Consideration of the critical points of the particle path pattern can lead to useful insights into the Reynolds number dependence of the flow. In this context it should be noted that while the ξ_0 coordinates of the critical points of both g_0 and g_∞ increase with Re, the values of p and q at the respective points are independent of Re. Thus the stable node of the Landau–Squire jet remains a stable node for all Reynolds numbers and the saddle of the unsteady dipole remains a saddle at all Reynolds numbers.

Neither of these flows is subject to transition as we shall define it shortly. This is consistent with the conclusions of Batchelor & Gill regarding the stability of the high-Reynolds-number limit of the Landau–Squire profile. What is important here is that, in a jet emanating from a constant source of momentum which is started at some initial time (and one may argue pro or con regarding the physical realizability of a uniformly steady jet), the flow at intermediate values of ξ must accommodate both the steady Landau–Squire behaviour at $\xi = 0$ and the unsteady dipole behaviour at $\xi = \infty$. If one accepts that the on-axis critical point moves to larger and larger values of ξ_0 as the Reynolds number is increased, then this would suggest that the stable node which would pertain at small Reynolds number (small ξ_0) cannot remain a stable node when the Reynolds number (and thus ξ_0) becomes large. Here the invariance of the particle trajectory pattern plays an important role, for it ensures that the type and character of a critical point is uniquely determined. Thus the node of the Landau–Squire jet cannot be changed to a saddle and, similarly, the saddle of the unsteady dipole cannot be changed to a node by merely referring the flow to a new observer. Stated another way, bifurcations produced by variation of the Reynolds number could not be simulated or removed by changing frames of reference.
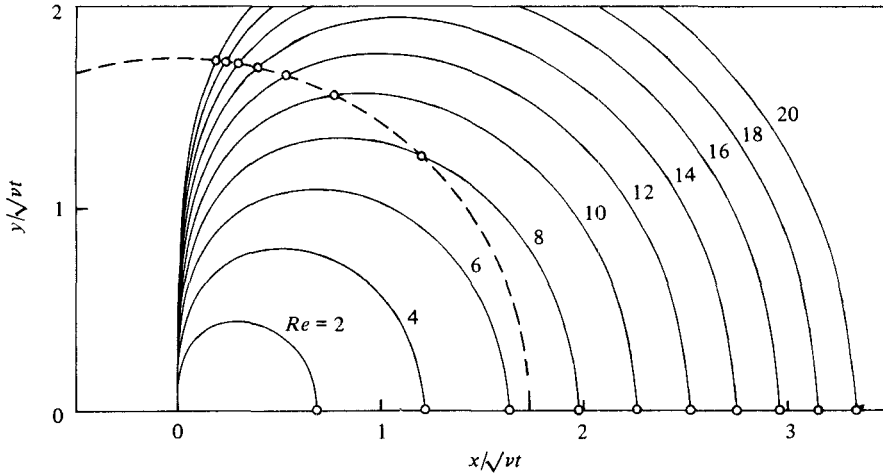
FIGURE 6. Zeros of the particle path equations for the low-Reynolds-number solution ((45) and (46)). Dashed line is the circle $\xi_0 = 1\cdot7633$. Solid lines are curves of (47) for various Reynolds numbers. Open circles are locations of critical points.

Let us now consider particle paths of the creeping flow solution (39). Upon substitution of (39) into (11) we have

$$\frac{d\xi}{d\tau} = \frac{Re^2}{2\pi}\frac{\cos\theta}{\xi^2}\left\{\frac{\xi}{2} - \frac{1}{\sqrt{\pi}}e^{-\frac14\xi^2} - \left(\frac{\xi}{2} - \frac{1}{\xi}\right)\operatorname{erf}\left(\tfrac12\xi\right)\right\} - \frac{\xi}{2}, \qquad (45)$$

$$\frac{d\theta}{d\tau} = \frac{-Re^2}{4\pi}\frac{\sin\theta}{\xi^2}\left\{\frac12 + \frac{1}{\xi\sqrt{\pi}}e^{-\frac14\xi^2} - \left(\frac12 + \frac{1}{\xi^2}\right)\operatorname{erf}\left(\tfrac12\xi\right)\right\}. \qquad (46)$$

Zeros of the right-hand side of (46) occur at ($\theta_0 = 0$ and π, all ξ) and ($\xi_0 = 1\cdot7633$, all θ). Setting the right-hand side of (45) equal to 0 gives

$$Re^2 = \frac{\pi\xi_0^3}{\left(\tfrac12\xi_0 - \pi^{-\frac12}e^{-\frac14\xi_0^2} - (\tfrac12\xi_0 - 1/\xi_0)\operatorname{erf}\left(\tfrac12\xi_0\right)\right)\cos\theta_0}. \qquad (47)$$

Equation (47) defines a family of curves in the (ξ_0, θ_0) plane of which several are drawn in figure 6. Superimposed on this family are the zeros of (45), i.e. the circle $\xi_0 = 1\cdot7633$ and the horizontal axis, $\theta_0 = 0$. Intersections in this figure locate the critical points of the system (45) and (46).

If $Re < 6\cdot7806$ there is a single node lying on the axis of the jet ($\theta_0 = 0$). In this Reynolds number range, equation (47) provides a relation between Re and ξ_0, the radial co-ordinate of the node which moves outward along the axis of the jet as Re is increased.

When Re exceeds $6\cdot7806$, the flow splits into three critical points; a saddle situated on the axis of the jet and two stable nodes located symmetrically about the axis at $\xi_0 = 1\cdot7633$ and

$$\theta_0 = \pm\,\cos^{-1}[(6\cdot7806/Re)^2]. \qquad (48)$$

As the Reynolds number is further increased, the nodes move away from the axis on the circle $\xi_0 = 1\cdot7633$. At the same time the ξ_0 coordinate of the saddle continues to
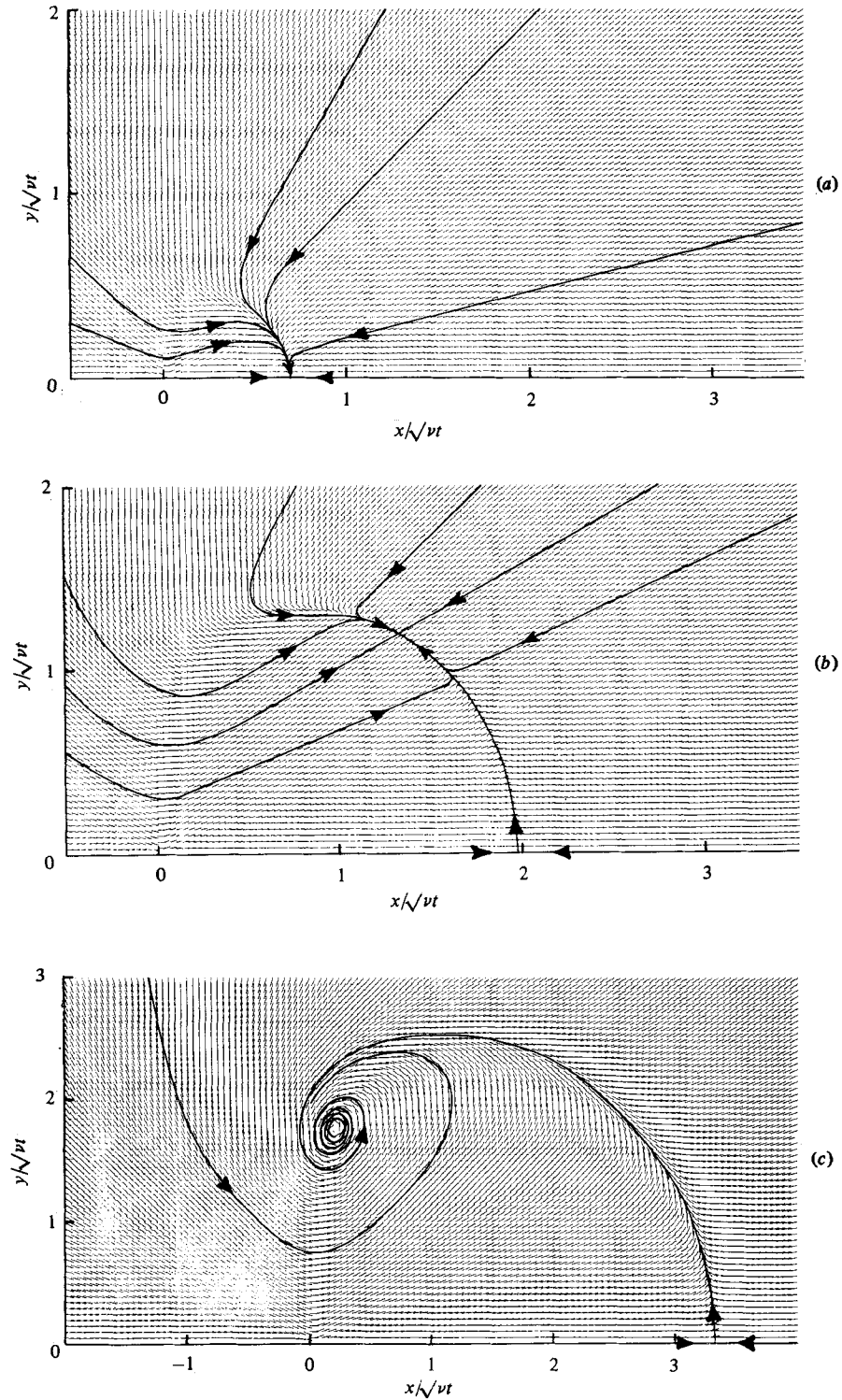
FIGURE 7. Particle trajectories for $G(\xi, \theta)$ at several Reynolds numbers
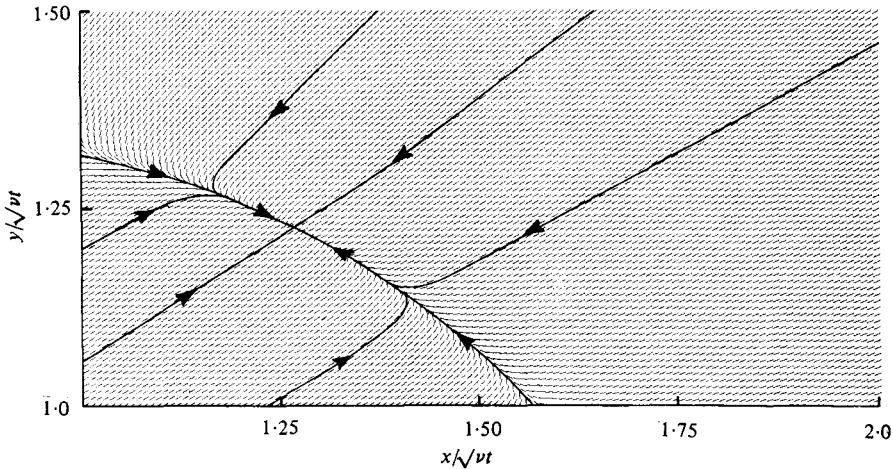(a) $Re = 2 \cdot 0$, (b) $Re = 8 \cdot 0$, (c) $Re = 20 \cdot 0$.

FIGURE 8. Particle trajectories for $G(\xi, \theta)$ at $Re = 8$ with increased
resolution near the off-axis critical point.

follow (47) with $\theta_0 = 0$. For the critical point on the axis, the invariants of the matrix of coefficients are

$$p_{\theta_0=0} = \frac{3}{2} - \frac{Re^2}{4\pi} \frac{1}{\xi_0^2} \left\{ \frac{1}{2} + \frac{1}{\xi_0 \sqrt{\pi}} e^{-\frac{1}{4}\xi_0^2} - \left(\frac{1}{2} + \frac{1}{\xi_0^2} \right) \operatorname{erf}\left(\tfrac{1}{2}\xi_0\right) \right\}, \tag{49}$$

$$q_{\theta_0=0} = (p_{\theta_0=0} - \tfrac{3}{2})(\tfrac{3}{2} - 2p_{\theta_0=0}). \tag{50}$$

For the critical point off the axis, the invariants are (ξ_0 evaluated as 1·7633)

$$p_{\theta_0 \neq 0} = \tfrac{3}{2}, \tag{51}$$

$$q_{\theta_0 \neq 0} = 6\cdot8143 \times 10^{-5} Re^4 - 0\cdot14405. \tag{52}$$

The off-axis node changes to a stable focus when $q_{\theta_0 \neq 0}$ exceeds $\frac{9}{16}$. This occurs at $Re = 10.09089$. Figures 7 and 8 depict the particle path pattern of (45) and (46) at Reynolds numbers in the three regimes of interest. The various patterns and their relation to the boundary conditions at $\xi = 0$ and $\xi = \infty$ are summarized schematically in figure 9 which shows the trajectory of the critical points of the creeping-flow solution in the (p, q) plane.

8. Discussion

It is interesting to contrast the complexity of figure 7 with the simplicity of some of the other variables which govern the flow. The reduced stream function (42) is symmetric in θ and simply scales with Re^2. Similarly, the vorticity

$$W(\xi, \theta) = \frac{Re^2}{4\pi} \sin \theta \left\{ \frac{1}{\xi^2} + \frac{1}{\xi\sqrt{\pi}} e^{-\frac{1}{4}\xi^2} - \frac{1}{\xi^2} \operatorname{erf}\left(\tfrac{1}{2}\xi\right) \right\}, \tag{53}$$

is also symmetric and scales with Re^2. A plot of $4\pi W / Re^2 \sin \theta$ in figure 10 reveals simply a rapidly decaying exponential. The point is that neither the vorticity nor the stream function show any special structure as the Reynolds number is increased. Whereas the behaviour of the fluid itself changes drastically. For example, the roll-up of particle trajectories depicted in figure 7(c) occurs entirely without any local concentration of
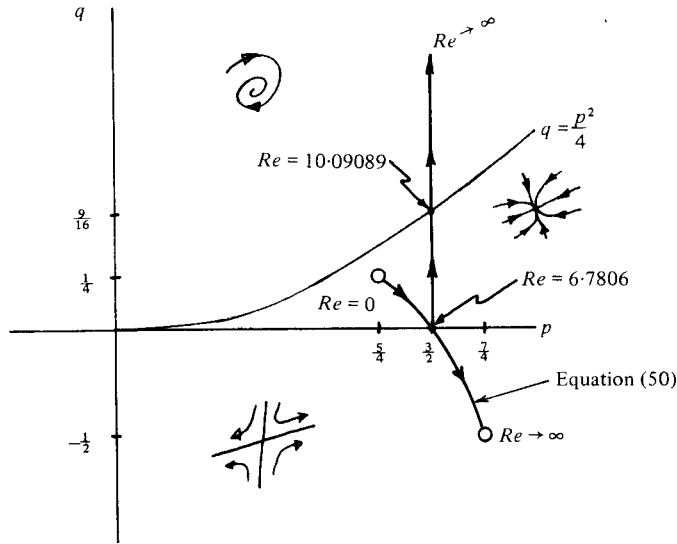
FIGURE 9. Trajectory of critical points of the system (45) and (46) in the (p, q) plane as Re is increased. Open circles correspond to values of (p, q) for the critical points of the boundary conditions at $\xi = 0$ and $\xi = \infty$.
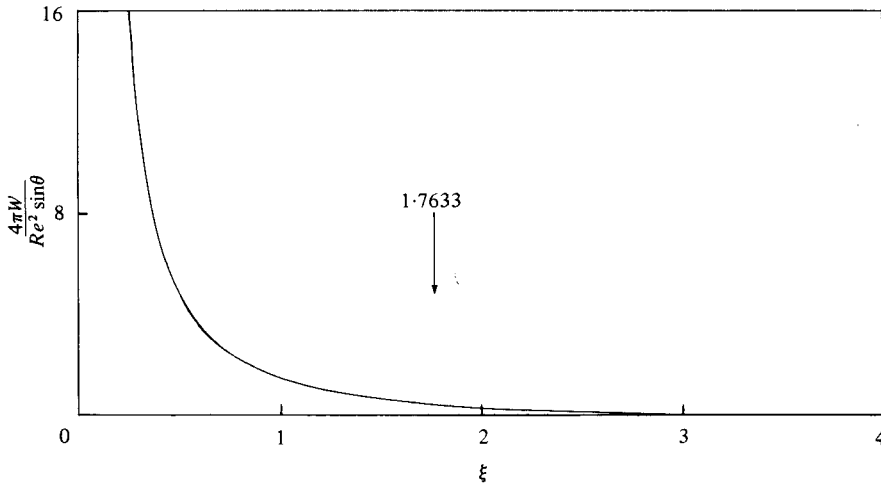

FIGURE 10. Vorticity derived from $G(\xi, \theta)$.

vorticity. The relevant quantity here is not the vorticity alone, but the combination of vorticity and strain given by (39). Moreover, the special values of Re at which changes in the flow pattern occur, come strictly from the analysis of particle paths. The source of asymmetry in the particle path pattern lies in the fact that the flow is directed outward along the positive x axis. It is this simple feature which leads to the possibility of critical points to the right of the origin but not to the left.

Many questions remain. The results of figure 7 lie outside the range of validity of the solution (34). Although it is probably fair to assume that the fully nonlinear solution would exhibit qualitatively similar behaviour, it is equally fair to expect significant

quantitative differences when the nonlinear terms are included. The sequence of events (node followed by saddle plus node, followed by saddle plus focus) is likely to be preserved, but the critical Reynolds numbers will be different from the values obtained from (45) and (46). That the sequence is preserved is virtually assured by the positions of the critical points of the bounding solutions in the (p, q) plane show in figure 9. To see this, consider the limiting values of p and q for the on-axis critical point of the creeping flow solution.

Equation (47) is used to remove Re^2 from (49) and (50). After taking limits of (49) and (50), we have for the creeping-flow solution

$$\lim_{\xi_0 \to 0} (p, q) = (\tfrac{5}{4}, \tfrac{1}{4}),$$

$$\lim_{\xi_0 \to \infty} (p, q) = (\tfrac{7}{4}, -\tfrac{1}{2})$$

Thus at low Reynolds numbers (small ξ_0), p and q approach the values for the Landau–Squire solution and at high Reynolds numbers (large ξ_0), p and q approach the values for the unsteady dipole. This is a consequence of the fact that the ξ_0 co-ordinate of the on-axis critical point increases monotonically with Reynolds number.

In the case of the on-axis critical point of the nonlinear solution, the zero Reynolds-number limit of course remains the same. The high-Reynolds-number limit is open to question. However, if one assumes that the radial coordinate, ξ_0, of the on-axis critical point increases with Reynolds number, then it is not unreasonable to assume that the nonlinear solution will also follow a trajectory in the (p, q) plane (figure 9) which takes it from $(p, q) = (\tfrac{5}{4}, \tfrac{1}{4})$ to $(p, q) = (\tfrac{7}{4}, -\tfrac{1}{2})$ as the Reynolds number increases from zero to infinity. Continuity requires that the trajectory intersect the horizontal axis at the intermediate point $(p, q) = (\tfrac{3}{2}, 0)$ and that the off-axis critical point move along the vertical line $p = \tfrac{3}{2}$. Thus, unless the nonlinear solution follows some very pathological trajectory in the (p, q) plane, the sequence node followed by saddle plus node followed by saddle plus focus, is likely to be preserved.

Some evidence that the nonlinear solution bifurcates can be found in the numerical results of Sozou & Pickering (1977). Their figures 1, 2 and 3 of instantaneous stream-lines at $Re = 2 \cdot 15$, $5 \cdot 90$ and $12 \cdot 5$, respectively, contain sufficient quantitative information ((*b*) and (*c*) of each figure) to look for off-axis critical points. In each figure, rays drawn through the origin tangent to the streamlines define a nearly semicircular curve of tangent points along which $V(\xi, \theta) = 0$. Differentiation of the stream function with respect to θ along this curve leads to a rough estimate of the angle at which $U(\xi, \theta) - \tfrac{1}{2}\xi$ equals zero. At $Re = 2 \cdot 15$ an off-axis critical point is not found. At $Re = 5 \cdot 90$, a critical point of the nonlinear solution lies at $(\xi_0, \theta_0) = (2 \cdot 0 \pm 0 \cdot 1, 11 \pm 1°)$.

Note that the creeping flow solution does not bifurcate until Re exceeds $6 \cdot 7806$. At $Re = 12 \cdot 5$, a critical point lies at approximately $(\xi_0, \theta_0) \simeq (2 \cdot 5 \pm 0 \cdot 1, 34 \pm 1°)$ compared to $(\xi_0, \theta_0) = (1 \cdot 7633, 72 \cdot 89°)$ for the creeping flow solution. Given the form of the particle trajectories at very low Reynolds numbers shown in figure 7(*a*), plus the lack of an off-axis critical point at $Re = 2 \cdot 15$, one may therefore conclude that the non-linear solution must bifurcate at least once at a critical Reynolds number between $2 \cdot 15$ and $5 \cdot 90$.

Experimental observations of jet transition are somewhat less certain. While the observations of transition at low Reynolds numbers by Viilu and Reynolds are

encouraging, neither experiment can be considered definitive. The fact is that any attempt to search for the critical points described in this paper would encounter considerable experimental difficulties. Most jets are created by the momentum flux associated with flow leaving a tube. The exit flow may have a parabolic or top hat profile or something in between. In any case, the initial development to a jet profile will take several jet diameters. If we consider a parabolic profile, as in the experiments of Viilu, then

$$\frac{(J/\rho)^{\frac{1}{2}}}{\nu} = \left(\frac{16\pi}{15}\right)^{\frac{1}{2}} \frac{UD}{\nu}, \tag{53}$$

where U is the mean tube exit velocity, and D is the tube diameter. The Reynolds number, based on x, of the free shear layer downstream of the tube exit is

$$Re_x = \left(\frac{15}{16\pi}\right)^{\frac{1}{2}} \left(\frac{x}{D}\right) \left(\frac{J}{\rho}\right)^{\frac{1}{2}} \Big/ \nu. \tag{54}$$

The Reynolds number of the jet and the Reynolds number of the shear layer are inextricably connected, with the Reynolds number at the end of the initial mixing zone $(x/D \simeq 6)$ several times the jet Reynolds number. The implication of this is that bifurcation of the developing jet is almost certain to be obscured by transition in the initial free shear layer.

Moreover, the constraint imposed by the dipole boundary condition at infinity is crucial to the transition process. Thus it may be important that the jet be produced by a force with a velocity perturbation at infinity proportional to $1/r^2$ and not by a source with a velocity perturbation which dies off like $1/r$. The injection of mass, no matter how small, will dominate the dipole behaviour at infinity, possibly changing the transition process in an essential way.

9. Concluding remarks

The main theme of this paper is the use of particle trajectories to reveal structural features associated with the Reynolds-number dependence of an axisymmetric jet. The analysis has led to several useful results. Transition in the unbounded jet is in the nature of transition in couette flow and occurs at specific critical values of the Reynolds number rather than in some range over which small disturbances are amplified. Moreover, the critical Reynolds numbers are small. Quite surprising is the complexity of the creeping flow solution which at first sight would appear to exhibit only a trivial dependence on Reynolds number.

The technique applied here is applicable to a rather general class of unsteady, self-similar flows (Cantwell 1979), both two-dimensional and three-dimensional. The way appears open to a rich variety of possible flow patterns and to an improved understanding of the manner in which increasing Reynolds number leads to increasing complexity of flow.

REFERENCES

ANDRONOV, A. A., LEONTOVICH, E. A., GORDON, I. I. & MAIER, A. G. 1971 *Theory of Bifurcations of Dynamic Systems on a Plane*. (Translated from Russian by D. Louvish.) Wiley. Israel Program for Scientific Translations, Jerusalem.

BATCHELOR, G. K. & GILL, A. E. 1962 Analysis of the stability of axi-symmetric jets. *J. Fluid Mech.* **14**, 529–551.

BENJAMIN, T. B. 1978 Bifurcation phenomena in steady flows of a viscous fluid. II. Experiments. *Proc. Roy. Soc.* A **359**, 27–43.

CANTWELL, B. J. 1979 Coherent turbulent structures as critical points in unsteady flow. *Arch. Mech. (Warsaw)* **31**, 707–721.

CANTWELL, B. J., COLES, D. E. & DIMOTAKIS, P. E. 1978 Structure and entrainment on the plane of symmetry of a turbulent spot. *J. Fluid Mech.* **87**, 641–672.

COLES, D. E. 1965 Transition in circular Couette flow. *J. Fluid Mech.* **21**, 385–425.

FENSTERMACHER, P. R., SWINNEY, H. L. & GOLUB, J. P. 1979 Dynamical instabilities and the transition to chaotic Taylor vortex flow. *J. Fluid Mech.* **94**, 103–128.

GILL, A. E. 1962 On the occurrence of condensations in steady axisymmetric jets. *J. Fluid Mech.* **15**, 557–567.

LANDAU, L. 1944 A new exact solution of Navier–Stokes equations. *C.R. Acad. Sci. Dok.* **43**, 286–288.

MA, A. S. C. & ONG, K. S. 1971 Impulsive-injection of air into stagnant surroundings. *IUTAM Symposium on Recent Research on Unsteady Boundary Layers*, **2**, 1952–1993.

PERRY, A. E. & FAIRLIE, B. D. 1974 Critical points in flow patterns. *Adv. Geophysics* **18**, 299–315.

REYNOLDS, A. J. 1962 Observations of a liquid-into-liquid jet. *J. Fluid Mech.* **14**, 552–556.

SCHUBAUER, G. B. & SKRAMSTAD, H. K. 1947 Laminar boundary layer oscillations and stability of laminar flow. *NACA War-Time Rep.* W-8 and *J. Aeronaut. Sci.* **14**, 69–78.

SOZOU, C. & PICKERING, W. M. 1977 The round laminar jet: the development of the flow field. *J. Fluid Mech.* **80**, 673–683.

SOZOU, C. 1979 Development of the flow field of a point force in an infinite fluid. *J. Fluid Mech.* **91**, 541–546.

SQUIRE, H. B. 1951 The round laminar jet. *Quart. J. Mech. Appl. Math.* **4**, 321–329.

TAYLOR, G. I. 1923 Stability of a viscous liquid contained between two rotating cylinders. *Phil. Trans. Roy. Soc.* A **223**, 289–343.

VIILU, A. 1962 An experimental determination of the minimum Reynolds number for instability in a free jet. *Trans. A.S.M.E.* E, *J. Appl. Mech.* **29**, 506–508.